Chapter 1

Beta Decay: Modes, Q-Values, and the Neutrino

> *"I have done something very bad today by proposing a particle that cannot be detected; it is something no theorist should ever do."*
>
> W. Pauli (1930), on the neutrino

Beta decay rearranges N and Z at fixed A through the weak interaction. When the neutron-to-proton ratio N/Z deviates from the value required for stability on the chart of nuclides, the nucleus can lower its mass by converting a neutron into a proton (β^- decay) or a proton into a neutron (β^+ decay or electron capture). This lecture develops the three decay modes with their full reaction equations (including neutrinos), derives Q-values first from nuclear masses and then from tabulated atomic masses (showing every electron term until it cancels), compares the energetics of β^+ and electron capture, and explains the continuous β spectrum that forced Pauli's neutrino hypothesis and Fermi's theory of β decay. The exposition follows Krane, Dunlap, and Demtröder [6, 1, 2, 5].

1.1 When the N/Z ratio is wrong

A stable nucleus requires a proper balance of neutrons and protons. For light nuclei the stable N/Z ratio is near unity; for heavy nuclei it rises toward ~ 1.5 because the Coulomb repulsion among protons must be compensated by extra neutrons [6, 1]. Two generic failures illustrate the logic:

1. **Excess of neutrons.** Consider $Z = 10$ with $N = 14$ on the stability line. If N increases to 16 while Z stays fixed, the N/Z ratio moves away from stability. A neutron inside the nucleus can convert to a proton, increasing Z by one and decreasing N by one. This is β^- decay.
2. **Excess of protons.** With the same $Z = 10$, $N = 14$ reference, suppose Z increases to 12 while N remains 14. Even though neutrons still outnumber protons, the proton count exceeds the stable value for this mass number. A proton converts to a neutron, decreasing Z by one. This is β^+ decay or electron capture.

Both conversions are mediated by the weak interaction. At the quark level the fundamental processes are

$$n \to p + e^- + \bar{\nu}_e, \qquad p \to n + e^+ + \nu_e, \qquad p + e^- \to n + \nu_e. \tag{1.1}$$

Electrons and positrons are not pre-existing constituents of the nucleus; they are created at the instant of decay, in contrast with α particles in α decay [6, 2].

1.2 Three modes of beta decay

For a parent nucleus ${}^A_Z X$ the three observed modes are:

Beta minus (β^-).

$$ {}^A_Z X \;\to\; {}^A_{Z+1}Y + e^- + \bar{\nu}_e. \tag{1.2}$$

The proton number increases by one; a neutron becomes a proton. The free neutron decays by this mode with mean lifetime $\tau_n \approx 879\,\mathrm{s}$, not half-life; the corresponding half-life is $t_{1/2} = \tau_n \ln 2 \approx 609\,\mathrm{s}$. Its energy release is $Q \approx 0.782\,\mathrm{MeV}$ [6, 20].

Beta plus (β^+).

$$ {}^A_Z X \;\to\; {}^A_{Z-1}Y + e^+ + \nu_e. \tag{1.3}$$

The proton number decreases by one. A *free* proton cannot undergo β^+ decay because the three-body final rest mass $m_n + m_e + m_\nu$ exceeds m_p. Inside a proton-rich nucleus, however, the change in nuclear binding energy can make the conversion exothermic. This does not imply decay of an isolated proton. Examples include ^{11}C and ^{18}F, used in positron-emission tomography [6, 1, 21].

Electron capture (EC).

$$ {}^A_Z X + e^- \;\to\; {}^A_{Z-1}Y + \nu_e. \tag{1.4}$$

The nucleus captures an atomic electron (usually from the K shell), converting a proton to a neutron. The daughter atom is left with a vacancy that fills by characteristic X-rays or Auger electrons. EC and β^+ both reduce Z by one and convert a proton to a neutron [6, 1].

Key idea

β^-: $Z \to Z+1$, antineutrino $\bar{\nu}_e$ emitted. β^+ and EC: $Z \to Z-1$, neutrino ν_e emitted. Free neutron decays; free proton does not. All three modes require a light, neutral, spin-$\frac{1}{2}$ neutrino (or antineutrino) to conserve energy, momentum, and angular momentum [6, 2].

Historical note

In December 1930 Wolfgang Pauli proposed an undetected neutral particle to save energy and angular momentum in β decay. Enrico Fermi named it the *neutrino* and built the first quantitative theory in 1934 [6, 2, 5]. Direct detection came only in 1956 (Reines and Cowan); today we distinguish ν_e from $\bar{\nu}_e$ in each decay mode as written above.

1.3 Q-value for β^-: nuclear masses, then atomic masses

Consider reaction (1.2). The Q-value is the difference between initial and final rest mass energies (excluding the negligible nuclear recoil):

$$Q_{\beta^-} = \Big[m'({}^A_Z X) - m'({}^A_{Z+1} Y) - m_e - m(\bar{\nu}_e)\Big]c^2, \tag{1.5}$$

where $m'(\cdot)$ denotes *nuclear* mass (nucleons only). The antineutrino mass is of order eV and is neglected: $m(\bar{\nu}_e) \approx 0$.

Step 1: express nuclear masses through atomic masses. Tables list *atomic* masses $m(\cdot)$ of neutral atoms. A neutral atom ${}^A_Z X$ contains the nucleus plus Z orbital electrons. Exactly, $m' = m - Zm_e + B_{\text{at}}/c^2$, where B_{at} is the positive total electronic binding energy. Neglecting the small B_{at}/c^2 mass correction for the present derivation,

$$m'({}^A_Z X) = m({}^A_Z X) - Zm_e. \tag{1.6}$$

For the daughter ${}^A_{Z+1} Y$, which has $Z+1$ electrons in its neutral atom,

$$m'({}^A_{Z+1} Y) = m({}^A_{Z+1} Y) - (Z+1)m_e. \tag{1.7}$$

Step 2: substitute into (1.5)**.**

$$\begin{aligned} Q_{\beta^-} &= \Big[(m(X) - Zm_e) - (m(Y) - (Z+1)m_e) - m_e\Big]c^2 \\ &= \Big[m(X) - Zm_e - m(Y) + (Z+1)m_e - m_e\Big]c^2. \end{aligned} \tag{1.8}$$

Step 3: collect electron terms. The electron mass terms are

$$-Zm_e + (Z+1)m_e - m_e = -Zm_e + Zm_e + m_e - m_e = 0. \tag{1.9}$$

Every explicit electron mass cancels. Therefore

$$Q_{\beta^-} = [m({}^A_Z X) - m({}^A_{Z+1} Y)]c^2, \tag{1.10}$$

using tabulated atomic masses directly [6, 1]. The energy Q_{β^-} is shared by the electron, antineutrino, and (negligibly) the recoiling daughter:

$$Q_{\beta^-} = K_e + E_\nu, \qquad K_{\max} \simeq Q_{\beta^-} \quad \text{(massless-neutrino, infinite-daughter-mass limit).} \tag{1.11}$$

For a parent at rest, the exact endpoint is obtained from relativistic energy–momentum conservation. If M_i and M_f are the consistently defined initial and daughter masses, then

$$K_{\max} = \frac{M_i^2 + m_e^2 - (M_f + m_\nu)^2}{2M_i}c^2 - m_e c^2. \tag{1.12}$$

For $M_f \gg m_e$, this is $K_{\max} \approx Q - m_\nu c^2 - p_{e,\max}^2/(2M_f)$. Thus the endpoint is slightly below Q

even for $m_\nu = 0$, because the daughter recoils.

Remark

Small differences in electronic binding between parent and daughter atoms (typically keV) are omitted above. Precision work sometimes retains them; for course estimates they are negligible compared with $Q \sim 1\text{–}3\,\text{MeV}$ [6].

1.4 Q-value for β^+: the $2m_ec^2$ threshold

For reaction (1.3), with nuclear masses and $m(\nu_e) \approx 0$,

$$Q_{\beta^+} = \Big[m'(X) - m'(Y) - m_e\Big]c^2, \tag{1.13}$$

where m_e is the positron mass ($m_{e^+} = m_{e^-}$). Using (1.6) with $m'(Y) = m(Y) - (Z-1)m_e$,

$$\begin{aligned} Q_{\beta^+} &= \Big[\big(m(X) - Zm_e\big) - \big(m(Y) - (Z-1)m_e\big) - m_e\Big]c^2 \\ &= \Big[m(X) - Zm_e - m(Y) + (Z-1)m_e - m_e\Big]c^2. \end{aligned} \tag{1.14}$$

Collecting electron terms:

$$-Zm_e + (Z-1)m_e - m_e = -Zm_e + Zm_e - m_e - m_e = -2m_e. \tag{1.15}$$

Hence

$$Q_{\beta^+} = [m(X) - m(Y)]c^2 - 2m_ec^2. \tag{1.16}$$

Positron emission requires not only $m(X) > m(Y)$ but

$$m(X) - m(Y) > 2m_e \quad\Longleftrightarrow\quad Q_{\beta^+} > 0, \tag{1.17}$$

with threshold $2m_ec^2 = 1.022\,\text{MeV}$. Typical β Q-values are only a few MeV, so this threshold is a substantial fraction of the available energy [6, 1].

1.5 Q-value for electron capture

With neutral-atom masses, the *atomic* EC Q-value is

$$Q_{\text{EC}}^{\text{atom}} = [m(X) - m(Y)]c^2. \tag{1.18}$$

This quantity is a property of the neutral parent and daughter ground states; one must not subtract a shell binding energy from its definition. For capture from shell i to a daughter nuclear level of excitation E_f^*, energy conservation instead gives the channel neutrino energy

$$E_{\nu,i} = Q_{\text{EC}}^{\text{atom}} - E_f^* - B_i - E_{\text{rec}}, \tag{1.19}$$

up to small differences associated with the final atomic configuration. Here B_i is the positive binding energy of the captured electron and $E_{\text{rec}} \simeq p_\nu^2/(2M_f)$. The daughter vacancy subsequently releases X rays and/or Auger electrons. Thus B_i lowers a particular neutrino-line energy, while the total energy release including atomic relaxation remains $Q_{\text{EC}}^{\text{atom}} - E_f^*$.

Caution

B_i is *not* universally a few eV. For K-shell capture in medium and heavy elements it can be tens of keV; for iodine, $B_K \approx 33.17\,\text{keV}$. Always use the binding energy of the shell from which capture occurs [6, 1].

Comparison of β^+ and EC. Subtracting (1.16) from the atomic EC Q-value,

$$Q_{\text{EC}}^{\text{atom}} - Q_{\beta^+} = 2m_e c^2 = 1.022\,\text{MeV}. \tag{1.20}$$

Whenever

$$0 < [m(X) - m(Y)]c^2 < 2m_e c^2, \tag{1.21}$$

electron capture is energetically allowed ($Q_{\text{EC}}^{\text{atom}} > 0$) for at least one accessible shell and daughter state, but positron emission is forbidden ($Q_{\beta^+} < 0$). This situation is common for moderately proton-rich nuclei [6, 1, 20].

Key idea

Atomic-mass formulas: $Q_{\beta^-} = [m(X) - m(Y)]c^2$, $Q_{\beta^+} = [m(X) - m(Y) - 2m_e]c^2$, $Q_{\text{EC}}^{\text{atom}} = [m(X) - m(Y)]c^2$. EC is favored over β^+ by exactly $2m_e c^2$ at the atomic Q-value level. For capture from shell i, however, $E_{\nu,i} = Q_{\text{EC}}^{\text{atom}} - E_f^* - B_i - E_{\text{rec}}$.

1.6 Continuous spectrum: ^{64}Cu and the missing energy

The Q-value appears as kinetic energy shared among the light decay products. The recoiling daughter nucleus carries negligible energy ($\sim$ keV or less). For β^- decay the electron and antineutrino share Q_{β^-}; neither body is at rest in general, so the electron kinetic energy K_e is *continuous* from near zero up to $K_{\max} \approx Q$.

Copper-64 is a remarkable laboratory example: it decays by both β^- and β^+ (and EC), so both spectra in Figs. 1.1 and 1.2 can be measured on one isotope [1, 21].

In the 1920s, before the neutrino was known, a *discrete* electron line was expected. If only the electron and heavy daughter emerged, two-body kinematics would fix the electron energy (as in α decay). Calorimetric experiments showed that the continuous distribution is intrinsic to the decay, not caused by energy loss in the source [6, 2]. Electrons were often observed with kinetic energy well below Q: where was the missing energy?

Pauli's solution (1930): a second, electrically neutral, highly penetrating particle carries away the "missing" energy and spin. Fermi (1934) incorporated the neutrino into a quantitative theory. The continuous spectrum is therefore a *three-body* phase-space effect, not an experimental artefact [6, 2, 5].

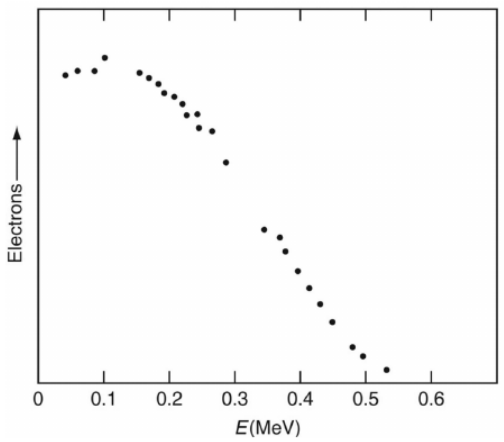

Figure 1.1: Energy spectrum of electrons from β^- decay of ^{64}Cu to ^{64}Zn. The endpoint near 0.58 MeV equals Q_{β^-} for the ground-state transition. Data from Langer, Moffat, and Price [29], as reproduced in Dunlap [1, 6].

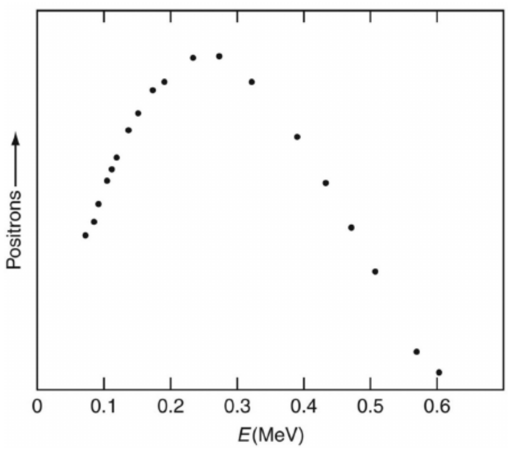

Figure 1.2: Energy spectrum of positrons from β^+ decay of ^{64}Cu to ^{64}Ni. Endpoint near 0.65 MeV. Same experimental reference as Fig. 1.1 [29, 1, 6].

Caution

The continuous spectrum is three-body kinematics, not instrumental smearing. The endpoint energy measures Q (and, in precision experiments near the endpoint, constrains the neutrino mass; see Lecture 19). Internal conversion and atomic effects can add low-energy structure, but the broad envelope is phase space [6, 14].

1.7 Toward Fermi theory: golden rule and plane-wave leptons

Fermi treated the weak interaction as a small perturbation on nuclear states. The transition rate from initial state ψ_i to final state ψ_f is Fermi's golden rule [6, 1, 14]:

$$\lambda = \frac{2\pi}{\hbar} \left|\langle\psi_f|H_{\text{int}}|\psi_i\rangle\right|^2 \frac{\mathrm{d}n}{\mathrm{d}E_f}, \tag{1.22}$$

where $\mathrm{d}n/\mathrm{d}E_f$ is the density of final states. For β^- decay,

$$\psi_i = \psi_p, \qquad \psi_f = \psi_d\, \psi_e\, \psi_\nu, \tag{1.23}$$

with ψ_p and ψ_d the parent and daughter nuclear wave functions.

The electron and antineutrino are treated as free plane waves normalized in volume V:

$$\psi_e(\boldsymbol{r}) = \frac{1}{\sqrt{V}} e^{i\boldsymbol{p}_e\cdot\boldsymbol{r}/\hbar} = \frac{1}{\sqrt{V}} \left(1 + \frac{i\boldsymbol{p}_e\cdot\boldsymbol{r}}{\hbar} + \cdots\right), \tag{1.24}$$

and similarly for ψ_ν. For typical β momenta ($p \sim 1\,\text{MeV}/c$) and nuclear radius $R \sim 5\,\text{fm}$, the dimensionless parameter $pR/\hbar \sim 0.03 \ll 1$. The *allowed* approximation keeps only the constant term ($\ell = 0$ for the lepton pair). The nuclear physics is then absorbed into a matrix element M_{fi} nearly independent of lepton energy, and the spectrum shape comes entirely from the lepton phase space developed in Lecture 19 [6, 1].

Key idea

Students should remember:

- Wrong $N/Z \Rightarrow \beta^-$ (neutron rich) or β^+/EC (proton rich).
- Free neutron decays; free proton does not ($m_n > m_p$).
- Atomic-mass $Q_{\beta^-} = [m(X) - m(Y)]c^2$; all electron masses cancel.
- Q_{β^+} has an extra $-2m_ec^2$; EC is $\approx 1.022\,\text{MeV}$ more favorable.
- Continuous spectrum $\Rightarrow$ three bodies $\Rightarrow$ neutrino.
- Golden rule: rate $\propto |M_{fi}|^2\times$ (phase space).

1.8 Deeper physics: Q_β, the continuous spectrum, and the neutrino

1.8.1 Energy release in β^- decay

For β^- decay $X \to Y + e^- + \bar{\nu}_e$, the nuclear Q-value follows the same mass-difference pattern as α decay,

$$Q_{\beta^-} = [M(X) - M(Y)]c^2, \tag{1.25}$$

using atomic masses of neutral atoms [6, 1]. The electron and antineutrino share this energy continuously because the three-body final state has a continuum of momentum partitions. The electron kinetic energy K therefore spans $0 \le K \le Q$ (minus small recoil and atomic binding corrections). A discrete line at $K = Q$ would imply a two-body final state; its absence led Pauli to postulate the neutrino [2, 14].

Free neutron decay

The simplest case is $n \to p + e^- + \bar{\nu}_e$ with $Q_{\beta^-} \approx 0.782\,\mathrm{MeV}$ [6, 20]. The measured mean lifetime $\tau_n \approx 879\,\mathrm{s}$ maps to $t_{1/2} \approx 609\,\mathrm{s}$. Proton recoil lowers the electron endpoint by only $\sim 0.1\,\mathrm{keV}$, negligible on the MeV scale. This decay is the laboratory standard for testing the V-A structure of the weak interaction [2].

1.8.2 Why the spectrum is continuous

In a two-body decay (for example α emission) energy and momentum fix the final kinetic energies uniquely. In β decay there are three light final particles. For fixed electron momentum p_e, the antineutrino can carry any momentum consistent with energy conservation, so many final configurations share the same K but differ in neutrino energy. Fermi's golden rule (Lecture 19) counts these configurations: the available phase volume grows with K and with $(Q - K)$ when $m_\nu = 0$, producing the characteristic rising-then-falling spectrum [6, 14].

Remark

Electron capture (EC) competes with β^+ emission when $Q_{\mathrm{EC}} > 0$. The observable Q for EC is reduced by the binding energy of the captured atomic electron, typically tens of keV. For heavy nuclei the continuous β spectrum shape is unchanged in principle, but atomic and chemical effects modify the low-energy end [1, 6].

Key idea

From spectrum shape to Fermi theory. The continuous β spectrum is not an experimental artefact: calorimetric measurements on ^{210}Bi confirmed that the electrons themselves carry a continuum of energies [1]. Lecture 19 converts this observation into a quantitative phase-space formula and Kurie plots that separate nuclear matrix elements from kinematics [6].

1.8.3 Limits of the two-body analogy

Unlike α decay, β spectra depend on the weak interaction structure (V-A) and on atomic Coulomb corrections $F(Z,K)$. The endpoint $K_{\max} \approx Q$ is robust, but the shape near $K = 0$ is modified for high-Z emitters because the Coulomb field favours low-energy electrons in β^- decay [6, 1]. Neutrino mass $m_\nu \neq 0$ replaces $(Q-K)^2$ by $(Q-K)\sqrt{(Q-K)^2 - m_\nu^2 c^4}$ and shifts the endpoint to $Q - m_\nu c^2$; this effect is searched at the sub-eV scale in tritium decay [2, 14]. Double β decay bypasses the continuous spectrum when single β is blocked by mass parabola considerations (Lecture 5) [6, 5].

1.8.4 Angular correlation and the V-A structure

The Wu experiment on polarised ^{60}Co showed that β decay violates parity: electrons emerge preferentially opposite to the nuclear spin [2, 6]. This selects the V-A form of the weak current and explains why only left-handed neutrinos appear at low energy. The angular distribution modifies the spectrum shape beyond pure phase space but does not remove the continuum: even with parity violation, three-body kinematics allows a range of electron energies at fixed nuclear orientation [14, 5]. Positron emitters used in PET (^{11}C, ^{18}F) and β^- sources in radiotherapy rely on the same Q_β bookkeeping developed in this lecture [6, 1].

Electron capture competes with β^+ when Q_{EC} is small and binding energies favour capture. In stellar environments, continuum electron capture alters effective rates: a reminder that laboratory Q values are necessary but not always sufficient for astrophysical weak rates. Delayed-neutron branching ratios add another applied data need for reactor and r-process networks.

1.9 Further physics from the literature

Free neutron decay. The simplest β^- example is free neutron decay, $n \to p + e^- + \bar{\nu}_e$, with energy release about 0.782 MeV; proton recoil makes the exact electron endpoint slightly lower. The measured neutron mean lifetime is $\tau_n \approx 879$ s, corresponding to $t_{1/2} \approx 609$ s. These observables provide precise tests of the V-A structure of the weak interaction [6, 2, 20].

Double beta decay. When single β decay is blocked (for example, when the intermediate nucleus would have higher mass), some even–even nuclei can decay by double β decay. Two-neutrino double β ($2\nu\beta\beta$) has been observed; neutrinoless double β ($0\nu\beta\beta$), if found, would prove that neutrinos are Majorana particles and would constrain the absolute neutrino mass scale [6, 1, 14, 5].

Parity violation. The Wu experiment (1957) showed that β decay does not conserve parity: electrons are preferentially emitted opposite to the nuclear spin in polarised ^{60}Co decay. This established the V-A form of the weak current and explained why only left-handed neutrinos and right-handed antineutrinos appear in β decay at low energy [2, 5, 6].

Medical and geochemical applications. Positron emitters (^{11}C, ^{18}F) and β^- sources are used in PET and radiotherapy. The β^- decay of ^{14}C provides radiocarbon dating. EC of ^{40}K contributes to the Earth's internal heat [6, 1, 13].

From the literature

Dunlap emphasises that calorimetric measurements on ^{210}Bi proved the continuous spectrum is a property of the decay electrons themselves, not energy loss before detection [1]. Krane's Table 9.1 lists representative β^-, β^+, and EC processes with Q and half-lives for order-of-magnitude estimates [6].

1.9.1 From the continuous spectrum to Fermi phase space (Lecture 19)

Pauli's neutrino hypothesis explains energy and momentum conservation in three-body decay. Fermi theory makes the spectrum quantitative: for each electron kinetic energy K, the available neutrino energy is $Q - K$ (when $m_\nu = 0$), and the phase-space volume grows as $K^2(Q-K)^2$ in the non-relativistic limit [6, 14]. The rising low-energy part of the spectrum reflects increasing electron phase space; the fall near $K = Q$ reflects shrinking neutrino phase space. Coulomb correction $F(Z, K)$ distorts the shape for high-Z emitters but does not remove the continuum [1].

Endpoint shift from a finite neutrino mass

If $m_\nu c^2 = 1\,\text{eV}$, the electron endpoint moves from $K_{\max} = Q$ to $K_{\max} \approx Q - m_\nu c^2$. For tritium with $Q \approx 18.6\,\text{keV}$, a $1\,\text{eV}$ neutrino mass shifts the endpoint by $\sim 0.005\%$, requiring precision spectroscopy to resolve [2, 6]. The Kurie plot remains linear in K only when the phase-space factor $(Q-K)\sqrt{(Q-K)^2 - m_\nu^2 c^4}$ is used instead of $(Q-K)^2$.

1.9.2 β cascades toward reactions and reactors

Each fission fragment β-decays toward stability (Lecture 24), producing reactor antineutrinos and decay heat. The same continuous spectrum shapes reactor $\bar{\nu}_e$ flux calculations used in oscillation experiments [14, 2]. β-delayed neutron emission from rare isotopes links weak decay to (n, γ) reaction networks in the r-process (Lecture 22) [51]. Forbidden transitions and atomic effects can mimic sterile-neutrino distortions if not modelled before invoking new physics [48].

Key idea

Arc through the course. Continuous β spectra (Lecture 18) become Kurie plots and $\log ft$ values (Lecture 19), then γ cascades (Lecture 20), then compound-nucleus β-delayed processes in reactions and fission (Lectures 21–24). The weak interaction is the slow step in the solar pp chain (Lecture 26) [36, 6].

1.9.3 Reactor antineutrinos and the β-decay network

Each fission event produces neutron-rich fragments that β-decay toward stability with a broad distribution of Q_β values. The cumulative $\bar{\nu}_e$ flux is therefore a weighted sum of many continuous spectra, not a single Kurie line [14, 2]. Precision reactor oscillation experiments require forbidden transitions and quasi-degenerate fragment chains to be modelled at the few-percent level. β-

delayed neutron emission from exotic waiting-point nuclei links the same weak process to (n, γ) reaction networks in the r-process (Lecture 22) [51]. The neutrino hypothesis of Lecture 18 is therefore not historical background alone: it is the bookkeeping tool that makes three-body phase space calculable.

1.9.4 Medical and geochemical β sources

The β^- decay of ^{14}C with $Q_\beta \approx 156\,\text{keV}$ provides radiocarbon dating; electron capture in ^{40}K contributes to the Earth's internal heat budget [6, 1]. These applications use the integrated decay rate $\lambda = \ln 2/t_{1/2}$, not the spectrum shape, but the continuous spectrum confirms that each decay carries a variable electron energy. In reactor physics, fragment β chains after fission (Lecture 24) produce both decay heat and antineutrinos; the cumulative spectrum is a superposition of thousands of channels with different Q values and $\log ft$ strengths [35, 14]. Understanding the allowed spectrum of Lecture 18 is prerequisite to Fermi theory (Lecture 19) and to all precision weak-interaction work that follows.

1.10 Deeper reading: endpoints, neutrinos, and delayed neutrons

The continuous β spectrum and the neutrino hypothesis of Lecture 18 underwrite endpoint searches for the absolute neutrino mass and for sterile-neutrino distortions. Atomic final-state distributions in tritium and pile-up systematics in calorimetric ^{163}Ho experiments are modern versions of the same spectral-shape problem.

Beta-delayed neutron emission appears when Q_β exceeds S_n of the daughter: a direct link between Lecture 5 masses and Lecture 24 reactor delayed-neutron fractions. Always compute Q from atomic masses with the correct electron-mass bookkeeping before discussing spectral endpoints.

Kurie plots and endpoints

A Kurie plot linearises an allowed spectrum so the intercept reads Q. Detector response, screening, and forbidden shape factors curve that line. Endpoint neutrino-mass searches are battles against those systematics at the electronvolt level. Nuclear physicists contribute clean Q values from traps; atomic and detector physicists own much of the shape.

Reactor antineutrino connection

Reactor spectra fold fission yields (Lecture 24) with β branching ratios and spectral shapes from this chapter. Uncertainties in forbidden transitions near endpoints feed sterile-neutrino anomaly discussions. The continuous spectrum is therefore both fundamental and applied.

Endpoint arithmetic

Using atomic masses, compute Q_{β^-} for ^{14}C and Q_{EC} for a small-Q case such as ^{7}Be. Sketch the allowed spectrum shape $\propto pE(Q-E)^2$ for the former and discuss why capture dominates when positron emission is energetically closed or suppressed. Estimate the Kurie intercept shift for a 1 eV neutrino mass relative to a kilo-electronvolt-scale Q: the fractional effect is tiny, which is why endpoint experiments are heroic.

Tie delayed neutrons to Lecture 5: when $Q_\beta > S_n$(daughter), a branch can emit neutrons after β decay. That branch is nuclear structure plus mass arithmetic, and it feeds reactor control data in Lecture 24.

The continuous β spectrum forced the neutrino's invention and still anchors endpoint mass experiments. Nuclear Q values are the indispensable calibration.

In practice, rework one numerical estimate from the lecture with a different parameter set and compare the shift to the quoted experimental uncertainty. If the shift exceeds the uncertainty, the estimate is teaching a scale, not delivering a fit. That distinction keeps theoretical cartoons honest when they sit beside evaluated data tables and modern many-body calculations. Along the course arc, write one sentence linking this chapter backward and one forward: the discipline of those two sentences is as important as any single formula. Examination problems rarely ask for a literature review, but they do ask for the scale argument that literature reviews presuppose.

Synthesis problem

Write a half-page note that (i) restates the chapter's central scale or selection rule in one equation, (ii) evaluates it numerically for one concrete nucleus or energy, and (iii) names the neighbouring lecture that uses the result. Keep the note free of research-frontier speculation; the goal is fluency with the lecture physics itself. If an assumption fails (Born approximation, spherical mean field, allowed transition, one-dimensional barrier), state the failure mode in a final sentence. That habit converts passive reading into examination-ready understanding and makes the later research-frontier box read as an extension rather than a replacement.

Research frontier: precision β decay and student projects

The continuous β spectrum and neutrino hypothesis of Lecture 18 underpin today's searches for the absolute neutrino-mass scale (tritium endpoint spectroscopy and ^{163}Ho calorimetry) and for sterile-neutrino spectral distortions. Rare-isotope beams enable β-delayed neutron spectroscopy that constrains r-process paths and reactor antineutrino inventories, while ultra-sensitive $0\nu\beta\beta$ experiments use the same weak-interaction language at a deeper level [48, 49, 51]. Atomic-mass Q values from traps remain the cleanest absolute energy calibrations for these programmes. Open issues include atomic final-state distributions in tritium, incomplete β-delayed neutron branching ratios for exotic precursors, and the nuclear-matrix-element bottleneck for interpreting a future $0\nu\beta\beta$ signal as a Majorana mass. Community roadmaps rank ton-scale double-beta experiments among the highest-priority construction projects [52].

Reactor antineutrino spectra and sterile-neutrino searches add applied motivation for precision β shapes. Forbidden transitions and atomic effects can mimic sterile-neutrino distortions if not modelled carefully. The lecture Kurie analysis is the right starting point for understanding why those systematics matter.

Atomic final-state effects and forbidden shape factors must be controlled before a spectral distortion is attributed to new neutrino physics.
Connecting those applied spectra back to the lecture continuous beta-spectrum derivation keeps the physics organised.
Student directions. (1) Data exercise: compute Q_{β^-} from atomic masses for ^{14}C and ^{37}Ar electron capture. (2) Sensitivity estimate: estimate the Kurie endpoint shift corresponding to a 0.5 eV neutrino mass in tritium. (3) Literature note: summarise one β-delayed neutron measurement relevant to reactor antineutrino anomalies or r-process waiting points.

1.11 Problems with solutions

Problem 18.1 — Derive Q_{β^-} from atomic masses

Show step by step that for ${}^A_ZX \to {}^A_{Z+1}Y + e^- + \bar{\nu}_e$,

$$Q_{\beta^-} = [m({}^A_ZX) - m({}^A_{Z+1}Y)]c^2, \tag{1.26}$$

starting from nuclear masses and neglecting $m(\bar{\nu}_e)$ and electronic binding [6].

Step-by-step

Step 1. Write the nuclear-mass Q-value:

$$Q_{\beta^-} = [m'(X) - m'(Y) - m_e]c^2.$$

Step 2. Relate nuclear and atomic masses:

$$m'(X) = m(X) - Zm_e, \qquad m'(Y) = m(Y) - (Z+1)m_e.$$

Step 3. Substitute:

$$Q_{\beta^-} = [m(X) - Zm_e - m(Y) + (Z+1)m_e - m_e]c^2.$$

Step 4. Simplify the electron terms:

$$-Zm_e + (Z+1)m_e - m_e = (-Z + Z + 1 - 1)m_e = 0.$$

Step 5. Conclude $Q_{\beta^-} = [m(X) - m(Y)]c^2$. All three electron masses (one in the daughter atom, one emitted, one subtracted explicitly) cancel identically [6, 1].

Problem 18.2 — β^+ threshold and EC window

The atomic mass excess of a parent exceeds that of the daughter by $\Delta m\, c^2 = 1.50$ MeV (parent heavier). Can the nucleus decay by β^+? By EC to the daughter ground state, first neglecting shell binding and recoil? What if $\Delta m\, c^2 = 0.80$ MeV?

Step-by-step

Case A: $\Delta m\, c^2 = 1.50\,\text{MeV}$.
$Q_{\beta+} = 1.50 - 1.022 = 0.48\,\text{MeV} > 0$: positron emission is allowed.
$Q_{\text{EC}}^{\text{atom}} = 1.50\,\text{MeV} > 0$: EC is also allowed. Neglecting recoil, capture from shell i gives $E_{\nu,i} \approx 1.50\,\text{MeV} - B_i$. Both modes compete; the atomic EC Q-value exceeds $Q_{\beta+}$ by $2m_ec^2$ [6, 1].
Case B: $\Delta m\, c^2 = 0.80\,\text{MeV}$.
$Q_{\beta+} = 0.80 - 1.022 = -0.22\,\text{MeV} < 0$: positron emission is forbidden.
$Q_{\text{EC}}^{\text{atom}} = 0.80\,\text{MeV} > 0$: EC is open provided an accessible shell and daughter level satisfy $B_i + E_f^* + E_{\text{rec}} < 0.80\,\text{MeV}$. This illustrates the window $0 < \Delta m\, c^2 < 2m_ec^2$ where EC alone occurs [1, 20].

Problem 18.3 — ^{64}Cu endpoint

Using atomic mass tables, estimate Q_{β^-} for $^{64}\text{Cu} \to {}^{64}\text{Zn} + e^- + \bar{\nu}_e$ and compare with the endpoint in Fig. 1.1.

Step-by-step

From ENSDF/NuDat [20, 21], the ground-state Q_{β^-} for ^{64}Cu is $0.579\,\text{MeV}$. Dunlap quotes $0.579\,\text{MeV}$ from atomic masses, in agreement with the Langer *et al.* spectrum endpoint near $0.58\,\text{MeV}$ (Fig. 1.1) [1, 6]. The equality $K_{\max} = Q$ holds only in the infinite-daughter-mass, massless-neutrino limit. In reality, $K_{\max} \approx Q - p_{e,\max}^2/(2M_f) - m_\nu c^2$, so recoil lowers the endpoint slightly. The spectrum falls to zero there because the neutrino phase space vanishes (derived fully in Lecture 19).

Problem 18.4 — Why is the spectrum continuous?

Explain in three sentences why α decay gives discrete α energies but β^- decay gives a continuous electron spectrum, even for a ground-state to ground-state transition.

Step-by-step

α decay is a two-body process (α + daughter nucleus). Energy and momentum conservation fix the α kinetic energy uniquely (up to small recoil corrections). β^- decay is a three-body process (electron + antineutrino + daughter). One continuous parameter (for example the antineutrino energy) remains undetermined, so the electron kinetic energy ranges continuously from 0 to Q [6, 2].

Bibliography

[1] R. A. Dunlap, *An Introduction to the Physics of Nuclei and Particles* (2nd ed.), IOP Publishing, Bristol (2023), DOI: 10.1088/978-0-7503-6094-4, Ch. 3 (Nuclear composition and size).

[2] W. Demtröder, *Nuclear and Particle Physics*, Undergraduate Lecture Notes in Physics, Springer, Cham (2023).

[3] S. Petrera, *Problems and Solutions in Nuclear and Particle Physics*, UNITEXT for Physics, Springer, Cham (2019).

[4] F. Terranova, *A Modern Primer in Particle and Nuclear Physics*, Oxford University Press (2021).

[5] S. D'Auria, *Introduction to Nuclear and Particle Physics*, Undergraduate Lecture Notes in Physics, Springer, Cham (2018).

[6] K. S. Krane, *Introductory Nuclear Physics*, Wiley, New York (1988).

[7] R. Hofstadter, "Electron scattering and nuclear structure," Rev. Mod. Phys. **28**, 214 (1956).

[8] H. F. Ehrenberg, R. Hofstadter, U. Meyer-Berkhout, D. G. Ravenhall, and S. E. Sobottka, "High-Energy Electron Scattering and the Charge Distribution of Carbon-12 and Oxygen-16," Phys. Rev. **113**, 666 (1959).

[9] H. Yukawa, "On the interaction of elementary particles. I," Proc. Phys.-Math. Soc. Japan **17**, 48 (1935).

[10] R. D. Woods and D. S. Saxon, "Diffuse surface optical model for nucleon-nuclei scattering," Phys. Rev. **95**, 577 (1954).

[11] H. G. J. Moseley, "The high-frequency spectra of the elements," Phil. Mag. **26**, 1024 (1913); **27**, 703 (1914).

[12] C. F. von Weizsäcker, "Zur Theorie der Kernmassen," Z. Phys. **96**, 431 (1935).

[13] P. Cappellaro, *Introduction to Applied Nuclear Physics* (MIT OpenCourseWare / LibreTexts), CC BY-NC-SA 4.0.

[14] J.-L. Basdevant, J. Rich, and M. Spiro, *Fundamentals in Nuclear Physics: From Nuclear Structure to Cosmology*, Springer, New York (2005).

[15] D. Tong, *Particle Physics*, Lecture notes (University of Cambridge / CERN school notes).

[16] M. G. Mayer, "On closed shells in nuclei. II," Phys. Rev. **75**, 1969 (1949).

[17] O. Haxel, J. H. D. Jensen, and H. E. Suess, "On the "magic numbers" in nuclear structure," Phys. Rev. **75**, 1766 (1949).

[18] T. Schmidt, "Über die magnetischen Momente der Atomkerne," Z. Phys. **106**, 358 (1937).

[19] L. W. Nordheim, "On spins, moments, and shells in nuclei," Phys. Rev. **78**, 294 (1950).

[20] Evaluated Nuclear Structure Data File (ENSDF), National Nuclear Data Center, Brookhaven National Laboratory, `https://www.nndc.bnl.gov/ensdf/`.

[21] NuDat 3, National Nuclear Data Center, Brookhaven National Laboratory, `https://www.nndc.bnl.gov/nudat3/`.

[22] N. J. Stone, "Table of nuclear magnetic dipole and electric quadrupole moments," At. Data Nucl. Data Tables **90**, 75 (2005); updated compilations at NNDC.

[23] W. N. Cottingham and D. A. Greenwood, *An Introduction to Nuclear Physics* (2nd ed.), Cambridge University Press, Cambridge (2001).

[24] H. Geiger and J. M. Nuttall, "The ranges of the α particles from the radioactive substances," Phil. Mag. **22**, 613 (1911).

[25] G. Gamow, "Zur Quantentheorie des Atomkernes," Z. Phys. **51**, 204 (1928).

[26] R. W. Gurney and E. U. Condon, "Wave mechanics and radioactive disintegration," Nature **122**, 439 (1928); Phys. Rev. **33**, 127 (1929).

[27] M. Wang, W. J. Huang, F. G. Kondev, G. Audi, and S. Naimi, "The AME 2020 atomic mass evaluation (II). Tables, graphs and references," Chin. Phys. C **45**, 030003 (2021).

[28] Laboratoire National Henri Becquerel (LNHB), Recommended decay data, `http://www.lnhb.fr/nuclear-data/nuclear-data-table/`.

[29] L. M. Langer, R. D. Moffat, and H. C. Price, Jr., "Low energy beta-ray spectra: P^{32} and Cu^{64}," Phys. Rev. **76**, 1725 (1949).

[30] L. M. Langer and H. C. Price, Jr., "Shapes of the beta-spectra of the forbidden transitions of Sb^{124}, Rb^{86}, Sr^{89}, Y^{91}, and Cs^{137}," Phys. Rev. **75**, 1769 (1949).

[31] D. C. Camp and L. M. Langer, "The shape of the ^{66}Ga positron spectrum and the contribution from $0^+ \to 0^+$ transitions," Phys. Rev. **129**, 1782 (1963).

[32] H. C. Verma, *Nuclear Physics: Fundamentals and Applications*, NPTEL/IIT Kanpur lecture series, `https://hcverma.in/ncl_phy_lectures`.

[33] International Atomic Energy Agency, *LiveChart of Nuclides*, evaluated structure, decay, reaction, and fission-yield data, `https://www-nds.iaea.org/relnsd/vcharthtml/VChartHTML.html`.

[34] T. Kibédi, T. W. Burrows, M. B. Trzhaskovskaya, P. M. Davidson, and C. W. Nestor, Jr., "Evaluation of theoretical conversion coefficients using BrIcc," Nucl. Instrum. Methods Phys. Res. A **589**, 202 (2008), DOI: 10.1016/j.nima.2008.02.051.

[35] D. A. Brown *et al.*, "ENDF/B-VIII.0: The 8th major release of the nuclear reaction data library with CIELO-project cross sections, new standards and thermal scattering data," Nucl. Data Sheets **148**, 1 (2018), DOI: 10.1016/j.nds.2018.02.001.

[36] B. Acharya *et al.*, "Solar fusion III: New data and theory for hydrogen-burning stars," Rev. Mod. Phys. **97**, 035002 (2025), DOI: 10.1103/8lm7-gs18.

[37] S. N. Ghoshal, "An experimental verification of the theory of compound nucleus," Phys. Rev. **80**, 939 (1950), DOI: 10.1103/PhysRev.80.939.

[38] D. Adhikari *et al.* (PREX Collaboration), "Accurate determination of the neutron skin thickness of ^{208}Pb through parity-violation in electron scattering," Phys. Rev. Lett. **126**, 172502 (2021), DOI: 10.1103/PhysRevLett.126.172502.

[39] B. T. Reed, F. J. Fattoyev, C. J. Horowitz, and J. Piekarewicz, "Implications of PREX-II on the equation of state of neutron-rich matter," Phys. Rev. Lett. **126**, 172503 (2021), DOI: 10.1103/PhysRevLett.126.172503.

[40] B. Hu *et al.*, "Ab initio predictions link the neutron skin of ^{208}Pb to nuclear forces," Nature Phys. **18**, 1196 (2022), DOI: 10.1038/s41567-022-01715-8.

[41] E. Epelbaum, H.-W. Hammer, and U.-G. Meißner, "Modern theory of nuclear forces," Rev. Mod. Phys. **81**, 1773 (2009), DOI: 10.1103/RevModPhys.81.1773.

[42] H.-W. Hammer, S. König, and U. van Kolck, "Nuclear effective field theory: Status and perspectives," Rev. Mod. Phys. **92**, 025004 (2020), DOI: 10.1103/RevModPhys.92.025004.

[43] T. Otsuka, A. Gade, O. Sorlin, T. Suzuki, and Y. Utsuno, "Evolution of shell structure in exotic nuclei," Rev. Mod. Phys. **92**, 015002 (2020), DOI: 10.1103/RevModPhys.92.015002.

[44] H. Hergert, S. K. Bogner, T. D. Morris, A. Schwenk, and K. Tsukiyama, "The in-medium similarity renormalization group: A novel ab initio method for nuclei," Phys. Rep. **621**, 165 (2016), DOI: 10.1016/j.physrep.2015.12.007.

[45] J. M. Lattimer and M. Prakash, "The equation of state of hot, dense matter and neutron stars," Phys. Rep. **621**, 127 (2016), DOI: 10.1016/j.physrep.2015.12.005.

[46] J. M. Lattimer, "Neutron stars and the nuclear matter equation of state," Annu. Rev. Nucl. Part. Sci. **71**, 433 (2021), DOI: 10.1146/annurev-nucl-102419-124827.

[47] B. P. Abbott *et al.* (LIGO Scientific Collaboration and Virgo Collaboration), "GW170817: Observation of gravitational waves from a binary neutron star inspiral," Phys. Rev. Lett. **119**, 161101 (2017), DOI: 10.1103/PhysRevLett.119.161101.

[48] M. J. Dolinski, A. W. P. Poon, and W. Rodejohann, "Neutrinoless double-beta decay: Status and prospects," Annu. Rev. Nucl. Part. Sci. **69**, 219 (2019), DOI: 10.1146/annurev-nucl-101918-023407.

[49] M. Agostini, G. Benato, J. A. Detwiler, J. Menéndez, and F. Vissani, "Toward the discovery of matter creation with neutrinoless $\beta\beta$ decay," Rev. Mod. Phys. **95**, 025002 (2023), DOI: 10.1103/RevModPhys.95.025002.

[50] P. Gysbers *et al.*, "Discrepancy between experimental and theoretical β-decay rates resolved from first principles," Nature Phys. **15**, 428 (2019), DOI: 10.1038/s41567-019-0450-7.

[51] H. L. Crawford, K. Fossez, S. König, and A. Spyrou, "A vision for the science of rare isotopes," Annu. Rev. Nucl. Part. Sci. **74**, 141 (2024), DOI: 10.1146/annurev-nucl-121423-091501.

[52] Nuclear Science Advisory Committee, *A New Era of Discovery: The 2023 Long Range Plan for Nuclear Science*, U.S. Department of Energy and National Science Foundation (2023), `https://nuclearsciencefuture.org/`.

[53] S. A. Giuliani, Z. Matheson, W. Nazarewicz, E. Olsen, P.-G. Reinhard, J. Sadhukhan, B. Schuetrumpf, N. Schunck, and P. Schwerdtfeger, "Colloquium: Superheavy elements: Oganesson and beyond," Rev. Mod. Phys. **91**, 011001 (2019), DOI: 10.1103/RevModPhys.91.011001.

[54] N. Schunck and D. Regnier, "Theory of nuclear fission," Prog. Part. Nucl. Phys. **125**, 103963 (2022), DOI: 10.1016/j.ppnp.2022.103963.

[55] I. Counts, J. Hur, D. P. L. Aude Craik, H. Jeon, C. Leung, J. C. Berengut, A. Geddes, A. Kawasaki, W. Jhe, and V. Vuletić, "Evidence for nonlinear isotope shift in Yb^+ search for new boson," Phys. Rev. Lett. **125**, 123002 (2020), DOI: 10.1103/PhysRevLett.125.123002.

[56] I. Angeli and K. P. Marinova, "Table of experimental nuclear ground state charge radii: An update," At. Data Nucl. Data Tables **99**, 69 (2013), DOI: 10.1016/j.adt.2011.12.006.

[57] S. Kraemer *et al.*, "Observation of the radiative decay of the ^{229}Th nuclear clock isomer," Nature **617**, 706 (2023), DOI: 10.1038/s41586-023-05894-z.